

# Flux Distribution in Superconducting Films with Holes

J. I. Vestgård, D. V. Shantsev, Y. M. Galperin and T. H. Johansen<sup>1</sup>

<sup>1</sup>*Department of Physics and Center for Advanced Materials and Nanotechnology,  
University of Oslo, P. O. Box 1048 Blindern, 0316 Oslo, Norway*

Flux penetration into type-II superconducting films is simulated for transverse applied magnetic field and flux creep dynamics. The films contain macroscopic, non-conducting holes and we suggest a new method to introduce the holes in the simulation formalism. The method implies reconstruction of the magnetic field change inside the hole. We find that in the region between the hole and the edge the current density is compressed so that the flux density is slightly reduced, but the traffic of flux is significantly increased. The results are in good agreement with magneto-optical studies of flux distributions in YBa<sub>2</sub>Cu<sub>3</sub>O<sub>x</sub> films.

PACS numbers: 74.25.Ha, 74.78.Bz, 74.25.Qt

## I. INTRODUCTION

The behavior of vortex matter in superconductors can to a large degree be controlled by introducing artificial defects. It has been known for a long time that randomly distributed defects, created e.g. by neutron irradiation, allow a dramatic enhancement of the critical current density,  $j_c$ . One may reach more specific goals by tuning the arrangement of artificial defects. In particular, experiments on superconducting thin films have revealed a large number of interesting effects, including matching effects,<sup>1</sup> noise reduction in SQUIDS,<sup>2</sup> rectified vortex motion,<sup>3,4</sup> anisotropy of  $j_c$ ,<sup>5</sup> and vortex guidance.<sup>6</sup>

In parallel with the experimental progress, the theoretical understanding of how artificially created patterns interact with vortex matter is also developing. Interaction between a single vortex and a cylindrical cavity in a bulk superconductor was considered within the London approximation in Ref. 7. This work extends the classical paper, Ref. 8, predicting the maximal number of flux quanta that can be trapped by a single hole. Current distribution around a 1D array of holes was calculated within the Ginsburg-Landau theory in Ref. 6. However, these theoretical works consider a *bulk* superconductor, while most experiments are on patterned *thin films*.<sup>1,2,3,4,5,6</sup> Moreover, a realistic model should take into account the strong pinning of vortices in the superconducting areas around the artificial defects. When the defect size is much larger than the London penetration depth, one can consider the average vortex density  $B$  rather than individual vortices. Such an approach was used in Ref. 9 to simulate flux penetration into a thin film with a 2D array of holes. It allowed to explain an asymmetrical flux penetration due to asymmetry in the hole shape. At the same time, the case of an individual hole in a thin film has not yet been carefully analysed. A main purpose of the present work is to acquire details of flux and current distributions in a superconducting strip with one individual hole.

An approximate picture of the current distribution around a non-conducting hole can be obtained within Bean's critical state model.<sup>10</sup> In the Bean model current stream lines are added from the edge with equal spac-

ing representing the critical current density. The presence of a hole forces the current to flow around it and hence pushes the flux front deeper into the sample. Both holes and sample corners give rise to so-called *d*-lines where the current changes direction discontinuously.<sup>11</sup> They are seen as dark lines<sup>12</sup> in images showing magnetic flux distributions.<sup>13,14</sup> For example, 90° corners give 45° straight *d*-lines<sup>15</sup> while semicircular indentations of the edge give parabolic *d*-lines.<sup>16</sup> The magneto-optical image of Fig. 1 shows *d*-lines spreading out from a circular hole towards the flux-free region. The same hole also introduces another pattern: a darkened region starting from the hole and extending *towards the edge*. This pattern is similar to the one observed by Eisenmenger et al., Ref. 17. The pattern does not fit with the common interpretation of the Bean model, which leaves the currents between the hole and the edge unperturbed. Ref. 17 discusses how to reinterpret the Bean model and explain the observed pattern as a second parabolic *d*-line. In this work, we will go further and do full dynamical simulations of flux penetration taking into account the non-local electrodynamics of films as well as flux creep. Our results provide details of flux and current distributions in the vicinity of a hole and suggest a new interpretation for the observed anomaly.

## II. MODEL

### A. Single-connected superconductors

Consider a type-II superconducting thin film placed in an increasing transverse magnetic field. The superconductor responds by generating screening currents to shield its interior. The current density is highest at the edges where the Lorentz force eventually overcomes the pinning force, leading to penetration of flux. According to the Bean model, the vortices move only when the local current density exceeds the critical value,  $j_c$ . A more realistic model for flux penetration also allows for flux creep at  $j < j_c$ . Macroscopically, flux creep is introduced

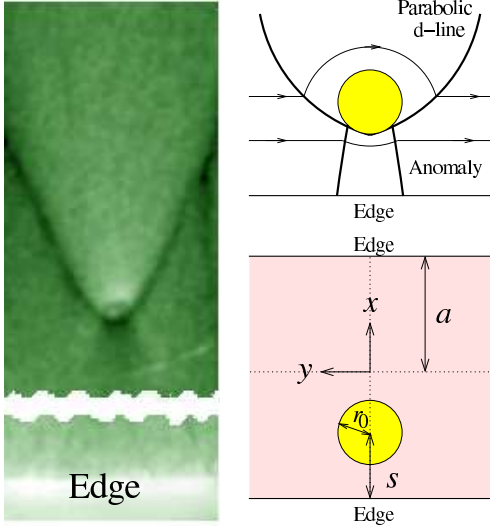


FIG. 1: Left: Magneto-optical image of  $B_z$  near a hole. Note the parabolic  $d$ -lines going upwards and a dark area going downwards from the hole. Right: a sketch of the strip with a circular hole indicating how peculiarities in the flux distribution are related to bending of the current stream-lines. Notations: film half-width is  $a$ , distance from the edge to the hole center is  $s$ , and the hole radius is  $r_0$ .

through a highly non-linear current voltage relation<sup>15,18</sup>

$$\mathbf{E} = \rho_0 \left( \frac{\mathbf{j}}{j_c} \right)^{n-1} \mathbf{j}, \quad (1)$$

where  $\mathbf{E}$  is electric field,  $\rho_0$  a resistivity constant,  $\mathbf{j}$  is current density, and  $n$  is the creep exponent. For thin films of  $\text{YBa}_2\text{Cu}_3\text{O}_x$ ,  $n$  is typically in the range from 10 to 70 depending on temperature and pinning strength.<sup>19</sup>

Flux dynamics of single-connected type-II superconductors in transverse geometry has been described thoroughly by E. H. Brandt. This work uses the same formalism and hence we only give a short summary of the simulation basics, mainly following Refs. 15,20 and 21. The next section will be devoted to additional changes for multiply-connected samples.

For films, it is a great simplification to work with the sheet current  $\mathbf{J}(\mathbf{r}) = \int_{-d/2}^{d/2} dz \mathbf{j}(\mathbf{r}, z)$ ,  $\mathbf{r} = (x, y)$ , in stead of the current density  $\mathbf{j}$ . This is justified as long as thickness,  $d$ , is small compared to the in-plane dimensions but much larger than the London penetration depth,  $\lambda$ . Finite  $\lambda$  can be handled with a small modification of the algorithm.<sup>21</sup> Since the current is conserved,  $\nabla \cdot \mathbf{J} = 0$ , it can be expressed as  $\mathbf{J} = \nabla \times \hat{z}g$ , where  $g = g(\mathbf{r})$  is the local magnetization.<sup>20</sup>

For single-connected thin films the Biot-Savart law can be formulated as

$$B_z(\mathbf{r}, z)/\mu_0 = H_a + \int_A d^2r' Q(\mathbf{r}, \mathbf{r}', z) g(\mathbf{r}'), \quad (2)$$

where  $H_a$  is the applied magnetic field, and  $A$  is the sample area. The kernel  $Q$  represents the field generated

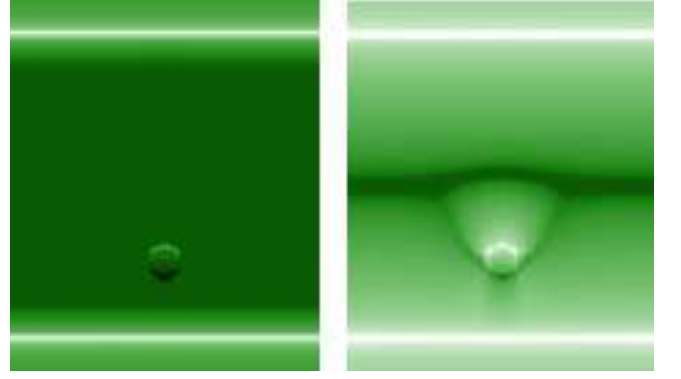


FIG. 2: Simulated magnetic field distribution in a long strip, plotted in the style of magneto-optical images, where the intensity represents  $B_z$ . At small applied field (left) the hole produces a field dipole and at large field (right) one can see the parabolic  $d$ -lines and a dark region between the hole and the edge, cf. the experimental image, Fig. 1;  $r_0/a = 0.1$ ,  $s/a = 0.5$ ,  $n = 19$ ,  $H_a/J_c = 0.2$  (left) and 1 (right), and  $\mu_0 \dot{H}_a = \rho_0 J_c / ad$ .

by a dipole of unit strength,<sup>15</sup>

$$Q(\mathbf{r}, \mathbf{r}', z) = \frac{1}{4\pi} \frac{2z^2 - (\mathbf{r} - \mathbf{r}')^2}{[z^2 + (\mathbf{r} - \mathbf{r}')^2]^{5/2}}. \quad (3)$$

We discretize the kernel on an equidistant grid with grid points  $r_i$  and weights  $w$  and obtain<sup>21</sup>

$$Q_{ij} = \delta_{ij} \left( C_i/w + \sum_l q_{il} \right) - q_{ij}, \quad (4)$$

where  $q_{ij} = 1/4\pi |\mathbf{r}_i - \mathbf{r}_j|^3$  for  $i \neq j$  and  $q_{ii} = 0$ . The function  $C$  depends on the sample geometry. It is given as

$$C(\mathbf{r}) = \int_{\text{outside}} \frac{dr'^2}{4\pi |\mathbf{r} - \mathbf{r}'|^3}. \quad (5)$$

The time evolution of  $g$  comes from the inverse of Eq. (2),

$$\dot{g}(\mathbf{r}) = \int_A d^2r' Q^{-1}(\mathbf{r}, \mathbf{r}') [\dot{B}_z(\mathbf{r}') - \mu_0 \dot{H}_a], \quad (6)$$

where  $Q^{-1}$  for discrete problem is the matrix inverse of Eq. (4).  $\dot{B}_z$  is given from Faraday's law as

$$\dot{B}_z(\mathbf{r}) = -(\nabla \times \mathbf{E})_z = \nabla \cdot \left( \frac{\rho}{d\mu_0} \nabla g \right), \quad (7)$$

with  $\rho = \rho_0 |\nabla g / J_c|^{n-1}$  obtained from Eq. 1. The right-hand side of Eq. (6) is expressed only via  $g$  and  $H_a$  so that time evolution of  $g$  can be found by integrating the equation numerically.

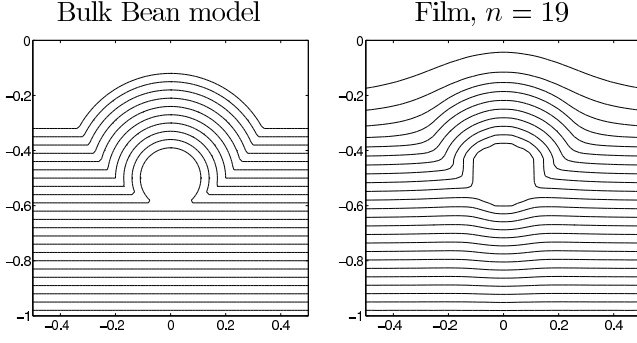


FIG. 3: The current stream lines for the bulk Bean model (left) and for film with finite  $n$  (right).

### B. Superconductors with holes

For macroscopic, arbitrarily shaped, single-connected, type-II superconducting films flux dynamics is fully described by Eq. (6). This basic equation can also be used for multiply connected samples, but in this case one needs to specify the dynamically changing value of  $g$  at the hole boundary. In Refs. 9 and 22 this value was set to the lowest value of  $g$  along the hole perimeter. This method turned out to be quite feasible but unfortunately it cannot reproduce the discussed pattern of Fig. 1. Moreover, it also introduces unphysical net flux into the hole before the flux front has reached it.

A completely different approach is to consider the holes as part of the sample, but ascribe to them a large Ohmic resistance or a strongly reduced  $J_c$ .<sup>23</sup> Then, Eq. (6) applies to the whole sample including the holes, while the material law, Eqs. (1) and (7), is spatially non-uniform. This approach is physically justified but numerically challenging due to huge electric field gradients. In addition, there still remain small but non-zero currents flowing within the holes.

In this work we propose a new approach that does not require any additional assumptions, though requires a larger computational time. In this approach the integration in Eq. (6) is extended over the whole sample area including the holes. Then the dynamics of  $g$  is described by the equation

$$\dot{g}(\mathbf{r}) = \int_A d^2r' Q^{-1}(\mathbf{r}, \mathbf{r}') [\dot{B}_z^{(s)}(\mathbf{r}') + \dot{B}_z^{(h)}(\mathbf{r}') - \mu_0 \dot{H}_a], \quad (8)$$

where  $A$  is the sample area including the hole. Here we presented  $\dot{B}_z$  as a sum  $\dot{B}_z^{(h)} + \dot{B}_z^{(s)}$  where  $\dot{B}_z^{(h)}$  is nonzero only in the hole and  $\dot{B}_z^{(s)}$  is nonzero within the superconducting areas.  $\dot{B}_z^{(s)}$  is calculated in the straightforward way using Eq. (7). The other term,  $\dot{B}_z^{(h)}$ , is defined by two conditions. The first condition is that current does not flow beyond the superconducting areas, i.e.,  $\dot{g}$  is constant within the hole. This constant is determined by the second condition, that the total change of magnetic flux inside the hole is related to the electric field at its

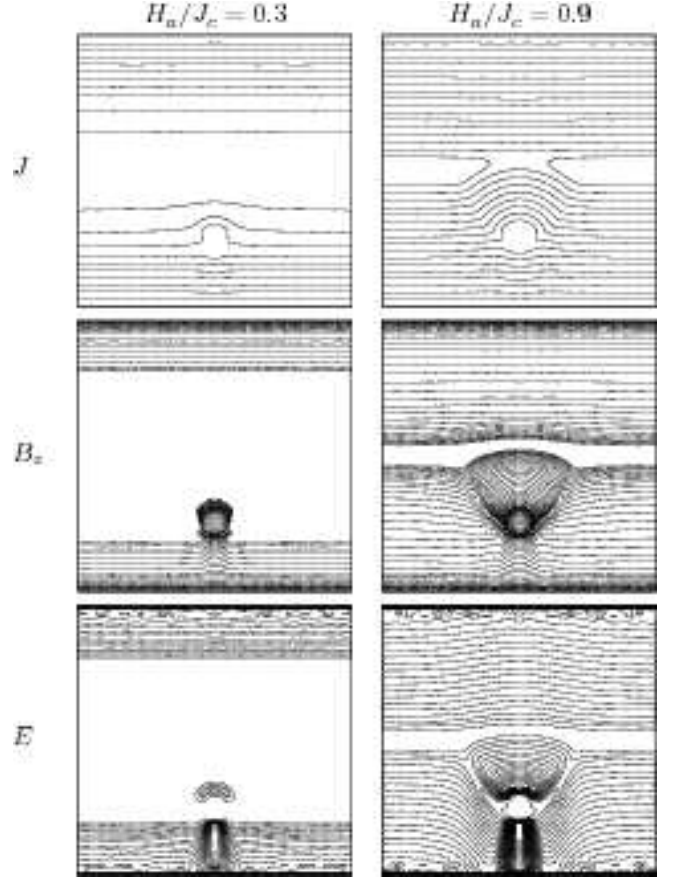


FIG. 4: Simulation results for a strip with a hole: the current stream lines (top),  $B_z$  contour lines (middle), and  $E$  contour lines (bottom). Note that the electric field is greatly enhanced in the channel between the hole and the edge;<sup>24</sup>  $H_a/J_c = 0.3$  and  $0.9$ . The remaining parameters are the same as for Fig. 2.

boundary through Faraday's law,

$$\int_{\text{hole}} d^2r \dot{B}_z = - \int_{\text{hole edge}} d\mathbf{l} \cdot \mathbf{E}. \quad (9)$$

In order to find a  $\dot{B}_z^{(h)}$  that satisfies the two conditions we use an iteration scheme. An initial guess,  $\dot{B}_z^{(h,0)}$ , is substituted into Eq. (8) to find  $\dot{g}^{(h,0)}$  inside the hole. The next approximation is found as

$$\dot{B}_z^{(h,1)}(\mathbf{r}) = \dot{B}_z^{(h,0)}(\mathbf{r}) - \int_{\text{hole}} d^2r' Q(\mathbf{r}, \mathbf{r}') \dot{g}^{(h,0)}(\mathbf{r}') + K, \quad (10)$$

where the constant  $K$  is chosen so that Eq. (9) is satisfied.  $\dot{B}_z^{(h,1)}$  is then inserted into Eq. (8) to find  $\dot{g}^{(h,1)}$ . This  $\dot{g}^{(h,1)}$  is in general non-uniform, but when the procedure is repeated  $\dot{g}^{(h,n)}$  becomes more uniform with every new iteration. A smart choice of the initial guess of  $\dot{B}_z^{(h,0)}$  is the final value at the previous time step,  $\dot{B}_z^{(h,0)}(\mathbf{r}, t) = \dot{B}_z^{(h,n)}(\mathbf{r}, t - \Delta t)$ . With this choice only a couple of iterations are sufficient.

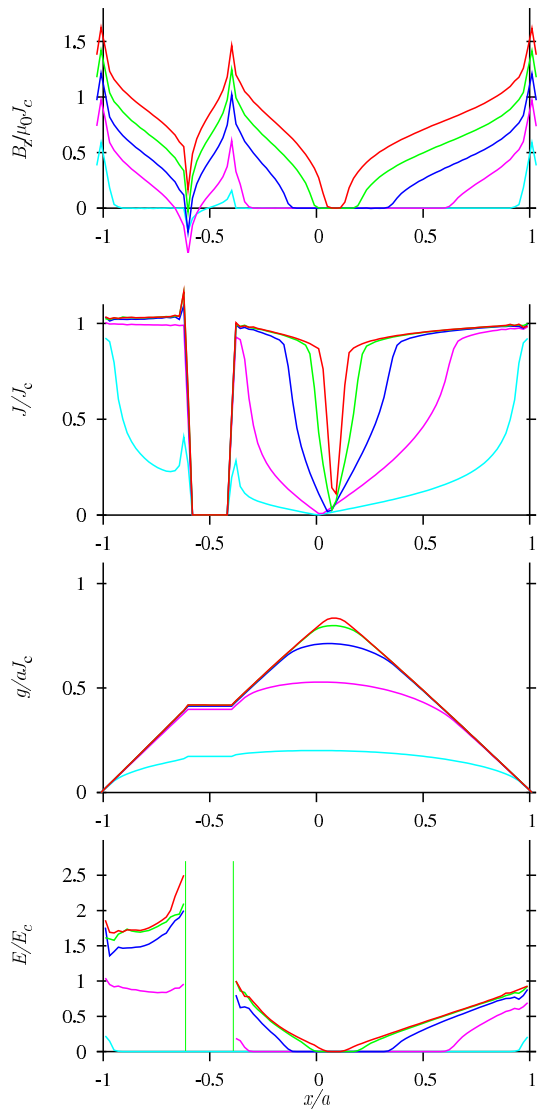


FIG. 5: Profiles of  $B_z$ ,  $J$ ,  $g$  and  $E$  through  $y = 0$  for a strip with a hole. The curves correspond to applied fields  $H_a/J_c = 0.1, 0.3, 0.5, 0.7$ , and  $0.9$ , and  $E_c = \rho_0 J_c/d$ . The remaining parameters are the same as for Fig. 2.

Note that the scheme presented here is in no way bound to the discrete formulation of the kernel, Eq. (4). It can be used for any formulation as long as both the forward and inverse relations between  $\dot{g}$  and  $\dot{B}_z$  are known. Further mathematical details are in appendix A.

### III. STRIP WITH A CIRCULAR HOLE

In this section, Eq. (8) is solved for an infinite superconducting strip in linearly increasing magnetic field. The strip is modeled using periodic boundary conditions in the  $y$ -direction, and examples of magnetic field distributions are given in Fig. 2. In the upper part one observes regular flux penetration with maximum of  $B_z$  at

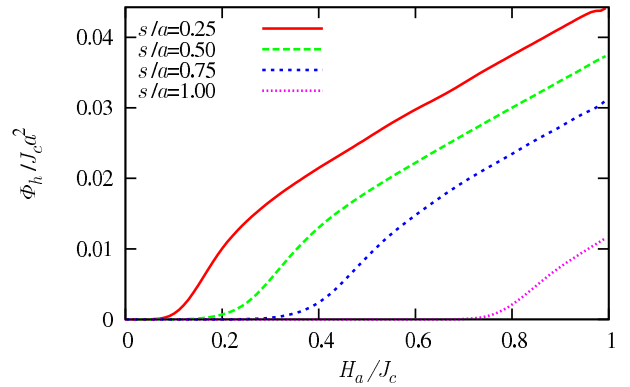


FIG. 6: Total flux inside the hole,  $\Phi_h = \int_{\text{hole}} d^2r B_z$ , as a function of  $H_a$ , for various distances  $s$  from the edge. For low fields  $\Phi_h$  is zero since the flux front has not reached the hole yet. For high fields  $\Phi_h$  grows linearly with  $H_a$  since the strip is saturated with  $J \approx J_c$ . Hole radii are  $r_0/a = 0.1$ . The remaining parameters are the same as for Fig. 2.

the edges. Flux penetration in the lower half is strongly affected by the presence a small, circular, non-conducting hole. Note that the flux distribution is perturbed in a region that significantly exceeds the hole dimensions.

The left image of Fig. 2 corresponds to a small field for which the flux front has not reached the hole yet. In this case the hole shows up as a field dipole, in agreement with magneto-optical observations; cf. Refs. 17 and 25. Namely, there is positive field at the farther side of the hole and a negative field at the side closer to the film edge. The negative fields shrinks when the flux front reaches the hole, but the asymmetry of the flux distribution inside the hole remains, as seen in the right image. As expected, the front becomes distorted so that the penetration is significantly deeper in the vicinity of the hole. For the full penetration image of Fig. 2 one also clearly see the  $d$ -lines as dark line originating at the hole and directed towards the middle of the strip. Such  $d$ -lines were first described in Ref. 11 within the Bean model framework and they are called  $d$ -lines because current changes direction discontinuously there. The discontinuity is most clearly seen in current stream line plot of Fig. 3 (left). For the Bean model,  $d$ -lines from circular holes are parabolic and by convention  $d$ -lines from small holes inside superconductors are often called parabolas. In the presence of flux creep the change of current direction is smeared as follows from Fig. 3 (right). However, the  $d$ -lines are still clearly visible, at least for  $n \gg 1$ .

Comparing the two panels of Fig. 3 we notice a qualitative difference between the current flow in the bulk Bean model and for films under the creep. In the Bean model the current density is everywhere constant and all the current that is blocked by the hole turns towards the strip center. The region between the hole and the edge is hence unaffected by the presence of the hole. For film creep dynamics this is no longer true and a certain fraction of the current will force its way here. As a result,



the current density is enhanced which is seen as denser stream lines in Fig. 3 (right). Since the stream lines bend they create the feature visible in the flux distribution of Fig. 2: a slightly darkened region starting at the hole and widening towards the edge. This feature can also be observed experimentally; cf. Fig. 1. It was analysed in detail in Ref. 17 and interpreted in terms of the Bean model as additional parabolic d-lines. Our experiment and simulations suggest a different interpretation. We believe that one should speak about an *area* of reduced flux density rather than new d-lines. Moreover, the appearance of this area is due to *locally enhanced* current density, hence it cannot be explained within the Bean model, postulating  $J = J_c$ . An enhanced current density also implies a strongly enhanced electric field. This is clearly seen in Fig. 4 showing the contour lines of  $E$ . A locally enhanced  $E$  means that there is an exceptionally intensive traffic of magnetic flux through the channel between the edge and the hole. The channel width is approximately given by the hole diameter, but increases slightly towards the edge. The width depends in general on the distance to the edge and the creep exponent  $n$ . Both larger distance and smaller  $n$  tend to make the channel wider.

After arrival to the hole, the flux is further directed in the fan-shaped region between the d-lines. Electric field within this region is also relatively high, again implying an intensive flux traffic. This situation is similar to the case of a semicircular indentation at the sample edge considered in Refs. 16, 26, and 27. The hole thus strongly rearranges trajectories of flux flow.

The above discussion is further confirmed by profiles of  $B_z$ ,  $J$ ,  $g$ , and  $E$  through the line  $y = 0$  shown in Fig. 5. The  $J$  profiles show features commonly observed in strips,<sup>28</sup> i.e., plateaus with values  $\sim J_c$  in the penetrated regions and shielding currents with  $J < J_c$  in the Meissner regions. The profiles show clearly the enhanced  $J$  and  $E$  between the edge and the hole. It is also interesting to see the negative  $B_z$  for low values and how the negative values gradually vanish when the main flux front gets in contact.

Fig. 6 shows the total flux in a circular hole,  $\Phi_h = \int_{\text{hole}} d^2r B_z$ , as a function of the applied field  $H_a$  for various distances between the hole and the edge. In the beginning,  $\Phi_h \approx 0$ , until the main flux front is in contact with the hole. Then it starts to increase. For high fields  $\Phi_h$  grows almost linearly with  $H_a$  at a universal growth rate determined by the hole area. The linear rate is not just the case for small holes in strips, but has also been found for e.g. ring geometry.<sup>29</sup> Note that for small fields  $\Phi_h$  is close to, but not exactly zero. The reason is the creation of two additional flux fronts: one positive towards the flux-free region and one negative towards the edge, as also seen in Fig. 5. Only when integrating  $B_z$  over a larger area that includes this additional penetration one finds that the total flux is exactly zero.<sup>30</sup> This integral is also a good consistency check of the boundary condition implementation, since a wrong value of  $g^{(h)}$  tends to

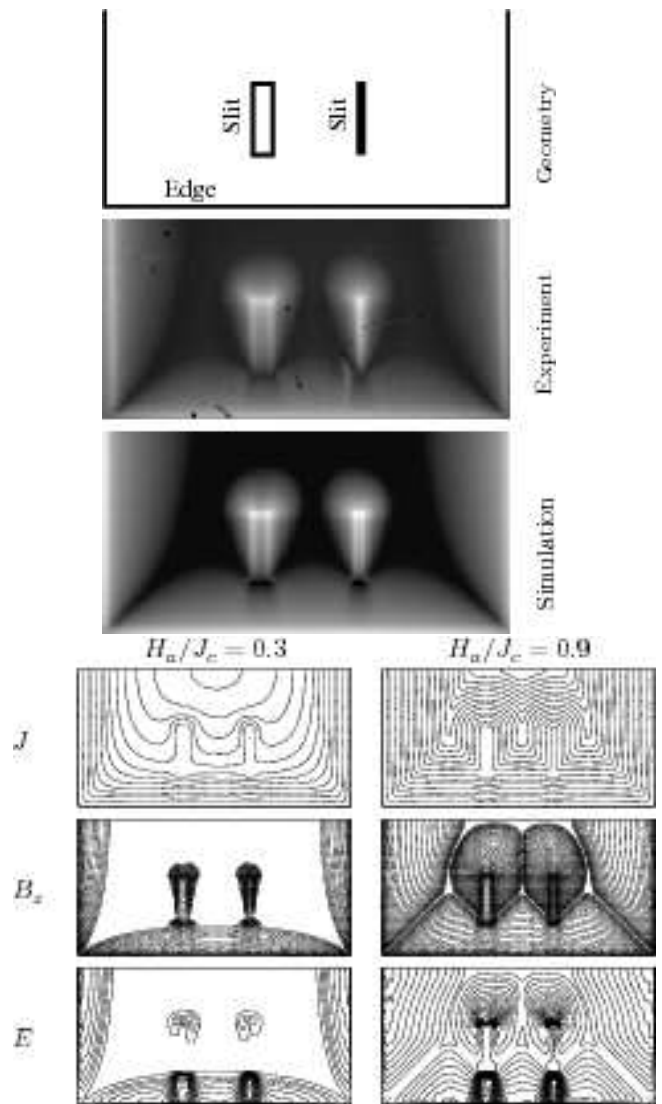


FIG. 7: A square with two slits (only the lower half is shown). Top: Sample sketch, experimental magneto-optical image of  $\text{YBa}_2\text{Cu}_3\text{O}_x$  film, and simulated magnetic field distribution. Bottom: current stream lines,  $B_z$  and  $E$  contour lines at  $H_a/J_c = 0.3$  and  $0.9$ , with  $n = 19$  and  $\mu_0 \dot{H}_a = \rho_0 J_c / ad$ . Note the strongly enhanced  $J$  and  $E$  between the slit and the edge and the complicated set of d-lines at full penetration.

introduce a net, unphysical flux in the hole.

#### IV. SQUARE WITH TWO SLITS

This section presents results of simulations of a square superconducting film with rectangular slits. The sample geometry is chosen to reassemble one particular  $\text{YBa}_2\text{Cu}_3\text{O}_x$  film and comparison of the simulation with a magneto-optical image of the sample is shown in Fig. 7. The experimental film thickness is 250 nm, and side lengths are 2.5 mm. The two slits have been cut out

with a laser. Details of the film preparation can be found elsewhere.<sup>31</sup>

The experiment and simulations show a great similarity both in large and in the details. The flux density is considerably enhanced everywhere along the slit edges, and reaches the maximal values at the upper corners. Our main result found for circular holes holds true also for rectangular slits. Namely, we again find a distinct dark region starting at the slit and widening towards the edge. It can be attributed to the over-critical current density in that region, which is clearly seen in the current stream-line plot. A new result for slits is a slightly brightened regions near the upper corners that appear due to concave current turns. A similar situation arises in superconductors of some other shapes having concave corners, e.g. in crosses.<sup>26</sup>

There also exist a few minor discrepancies between flux distributions obtained in the simulations and in the experiment of Fig. 7. The most notable is the details of the region of reduced  $B_z$  at the side of slits close to the edge. The values of  $B_z$  appear to be less in the simulation than in experiment. This might be caused by simplifications, like the disregarded  $B$ -dependency of the material law or the simplification of using the sheet current in stead of the true current density.

## V. SUMMARY

We have proposed a new method for treating boundary conditions of non-conducting holes inside macroscopic, type-II superconducting films. The key point is to reconstruct the at first unknown  $\vec{B}_z$  inside the holes, at each time step of the simulation. The method is capable of handling any number of holes of arbitrary shape.

The simulations of flux dynamics assuming a material law  $E \sim j^n$  reproduce very well flux distributions observed by magneto-optical imaging in  $\text{YBa}_2\text{Cu}_3\text{O}_x$  films, for circular holes as well as rectangular slits. In particular, they demonstrate a significant enhancement of current density in the region between a hole (slit) and the edge leading to a more intensive traffic of flux. This region appears darker in magneto-optical images due to a slight bending of current stream lines.

We thank C. Romero-Salazar and Ch. Jooss for fruitful discussions and M. Baziljevich for experimental data

on Fig 7. This work was supported financially by The Norwegian Research Council, Grant No. 158518/431 (NANOMAT) and by FUNMAT@UIO.

## APPENDIX A: NUMERICAL DETAILS

The simulations are run on a  $N \times N$  square grid. The creep exponent and the ramp rate are  $n = 19$  and  $\mu_0 \dot{H}_a = \rho_0 J_c / ad$ , a regime in which creep is low, but not negligible. Changing  $n$  would only do quantitative changes to the results. For small exponents the plateaus of current profiles, like Fig. 5, would be less flat and there would also be more current compressed between the holes and the edge.

The main limiting factor of the simulations is memory consumption since the kernel matrix  $Q$ , Eq. (4), has dimension  $N^2 \times N^2$ . The simulations are run with  $N = 100$  grid points, which yields a kernel matrix of dimension  $5000 \times 5000$ , when the sample symmetry has been exploited.<sup>15</sup>

The kernel  $Q$  in Eq. (4) depends explicitly on the sample shape. Since the strip is infinite in the  $y$ -direction,  $Q$  should be computed via an infinite sum over strip segments. However a good approximation is achieved with only one segment on each side of the “main” strip. The strip segments further away contain zero net current and the dipole like character means that they have a negligible effect. A good accuracy of this approximation was checked by comparing the Meissner state width,  $b$ , obtained for very high  $n$  with the analytical film Bean-model result,<sup>33</sup>  $b = a / \cosh(\pi H_a / J_c)$ .

The reconstruction of  $\vec{B}_z$  inside the hole, Eq. (10), need not use the full  $Q$  from Eq. (4). The best is to use a smaller kernel,  $\tilde{Q}$ , also generated with Eq. (4), but only including points inside the hole. Fast convergence of Eq. (10) is achieved by ignoring currents at the hole perimeter, which means that  $\tilde{Q}$  should use  $C(\mathbf{r}) = 0$ .

The most difficult numerical problem in our method is the calculation of the electric field at the boundary in Eq. (9). The electric field is given by the power law, Eq. (1), and is largely fluctuating between neighboring grid points. A stable way to handle this is to take the average of only the most significant values of  $E$  and use  $2\pi r$  and  $\pi r^2$  for the hole circumference and area.

<sup>1</sup> V. V. Moshchalkov, M. Baert, V. V. Metlushko, E. Rosseel, M. J. Van Bael, K. Temst, Y. Bruynseraede, and R. Jonckheere, Phys. Rev. B **57**, 3615 (1998).

<sup>2</sup> R. Wördenweber and P. Selders, Physica C **366**, 135 (2002).

<sup>3</sup> C. C. de Souza Silva, J. Van de Vondel, M. Morelle, and V. V. Moshchalkov, Nature **440**, 651 (2006).

<sup>4</sup> J. Van de Vondel, C. C. de Souza Silva, B. Y. Zhu, M. Morelle, and V. V. Moshchalkov, Phys. Rev. Lett **94**,

057003 (2005).

<sup>5</sup> M. Pannetier, R. J. Wijngaarden, I. Fløan, J. Rector, B. Dam, R. Griessen, P. Lahl, and R. Wördenweber, Phys. Rev. B **67**, 212501 (2003).

<sup>6</sup> R. Wördenweber, P. Dymashevski, and V. R. Misko, Phys. Rev. B **69**, 184504 (2004).

<sup>7</sup> H. Nordborg and V. M. Vinokur, Phys. Rev. B **62**, 12 408 (2000).

<sup>8</sup> G. S. Mkrtchyan and V. V. Shmidt, Sov. Phys. JETP **34**,

- 195 (1972).
- <sup>9</sup> D. G. Gheorghe, M. Menghini, R. J. Wijngaarden, S. Raedts, A. V. Silhanek, and V. V. Moshchalkov, *Physica C* **437-438**, 69 (2006).
  - <sup>10</sup> C. P. Bean, *Rev. Mod. Phys.* **36**, 31 (1964).
  - <sup>11</sup> A. M. Campbell and J. Evetts, *Critical Currents in Superconductors* (Taylor and Francis LTD, London, 1972).
  - <sup>12</sup> What is dark and bright in MO-images depends on experimental setup. In this paper dark means low field and bright high field, which is the most common situation.
  - <sup>13</sup> T. Schuster, M. V. Indenbom, M. R. Koblishka, H. Kuhn, and H. Kronmüller, *Phys. Rev. B* **49**, 3443 (1994).
  - <sup>14</sup> C. Jooss, J. Albrecht, H. Kuhn, S. Leonhardt, and H. Kronmüller, *Rep. Prog. Phys.* **65**, 651 (2002).
  - <sup>15</sup> E. H. Brandt, *Phys. Rev. B* **52**, 15442 (1995).
  - <sup>16</sup> R. G. Mints and E. H. Brandt, *Phys. Rev. B* **54**, 12421 (1996).
  - <sup>17</sup> J. Eisenmenger, P. Leiderer, M. Wallenhorst, and H. Dötsch, *Phys. Rev. B* **64**, 104503 (2001).
  - <sup>18</sup> E. Zeldov, N. M. Amer, G. Koren, A. Gupta, and M. W. McElfresh, *Appl. Phys. Lett.* **56**, 680 (1990).
  - <sup>19</sup> J. Z. Sun, C. B. Eom, B. Lairson, J. C. Bravman, and T. H. Geballe, *Phys. Rev. B* **43**, 3002 (1991).
  - <sup>20</sup> E. H. Brandt, *Phys. Rev. Lett.* **74**, 3025 (1995).
  - <sup>21</sup> E. H. Brandt, *Phys. Rev. B* **72**, 024529 (2005).
  - <sup>22</sup> K. A. Lörincz, M. S. Welling, J. H. Rector, and R. J. Wijngaarden, *Physica C* **411**, 1 (2004).
  - <sup>23</sup> A. Crisan, A. Pross, D. Cole, S. J. Bending, R. Wördenweber, P. Lahl, and E. H. Brandt, *Phys. Rev. B* **71**, 144504 (2005).
  - <sup>24</sup>  $E$  inside the hole cannot be found from the material law and is simply put to zero in the plots. The correct  $E$  inside the hole must be found from Faraday's law.<sup>32</sup>
  - <sup>25</sup> V. V. Yurchenko, R. Wördenweber, Y. M. Galperin, D. V. Shantsev, J. I. Vestgård, and T. H. Johansen, *Physica C* **437-438**, 357 (2006).
  - <sup>26</sup> T. Schuster, H. Kuhn, and E. H. Brandt, *Phys. Rev. B* **54**, 3514 (1996).
  - <sup>27</sup> J. I. Vestgård, D. V. Shantsev, Y. M. Galperin, and T. H. Johansen (2007), (Sent to *Phys. Rev. B*) arXiv:0706.0631.
  - <sup>28</sup> T. H. Johansen, M. Baziljevich, H. Bratsberg, Y. Galperin, P. E. Lindelof, Y. Shen, and P. Vase, *Phys. Rev. B* **54**, 16264 (1996).
  - <sup>29</sup> Å. A. F. Olsen, T. H. Johansen, D. Shantsev, E.-M. Choi, H.-S. Lee, H. J. Kim, and S.-I. Lee, *Phys. Rev. B* **76**, 024510 (2007).
  - <sup>30</sup> E. H. Brandt, *Phys. Rev. B* **55**, 14513 (1997).
  - <sup>31</sup> M. Baziljevich, T. H. Johansen, H. Bratsberg, Y. Shen, and P. Vase, *Appl. Phys. Lett.* **69**, 3590 (1996).
  - <sup>32</sup> C. Jooss and V. Born, *Phys. Rev. B* **73**, 094508 (2006).
  - <sup>33</sup> E. H. Brandt and M. Indenbom, *Phys. Rev. B* **48**, 12893 (1993).